Effect of carbon equivalent on thermal and mechanical properties of compacted graphite cast iron

Yangzhen Liu,[a] Jiandong Xing, Yefei Li,[b] Yong Wang, Lei Wang, and Baochao Zheng
State Key Laboratory for Mechanical Behavior of Materials, Xi'an Jiaotong University, Xi'an, Shaanxi, 710049, People's Republic of China

Dong Tao
School of Materials and Chemical Engineering, Xi'an Technological University, Xi'an, Shaanxi, 710021, People's Republic of China

The effects of carbon equivalent on thermal and mechanical properties of compacted graphite cast irons were investigated at ambient temperature, 300 and 500 °C, respectively. The group implied the change of carbon content to control the carbon equivalent. The results indicated that with the increasing carbon equivalent from 4.43 to 4.74, the graphite count increase. The thermal conductivity was 48.64, 44.55, 49.04, and 50.36 W/mK for carbon equivalent about 4.43–4.74 of compacted graphite cast irons at ambient temperature, respectively. With an increase in temperature, the thermal conductivity decrease. Moreover, with the increasing carbon equivalent, the tensile strength and yield strength increase initially, and then decrease at ambient temperature, 300 and 500 °C, respectively. With an increase in temperature, the tensile strength and yield strength decrease. Characterization of fracture surface indicated that the mixed ductile-brittle fracture mode prevailed in the compacted graphite cast irons with different carbon equivalents.

I. INTRODUCTION

The graphite morphology of compacted graphite cast iron (CGI) is a short, stubby, and wormlike form with rounded edges.[1–3] Owing to this type of structure, compacted graphite cast iron possesses special properties that are intermediate between gray and ductile cast iron. Previous works[4–7] have indicated that, the preparation of compacted graphite cast iron produce less dross and less susceptible to shrinkage porosity and carbide formation. Moreover, the strength, ductility, and toughness of compacted graphite cast iron are superior to gray iron and approach those of ductile iron. The thermal conductivity and damping capacity of compacted graphite cast iron are better than ductile iron. Based on aforementioned results, the compacted graphite cast iron, stemmed from the good combination of thermal and mechanical properties, is an excellent candidate in numerous industrial applications, such as ingot molds, brake drums, and cylinder heads.[8–10]

In the past decades, particular emphasis has recently been placed on the improvement of mechanical properties of compacted graphite cast iron.[11–20] The study by König et al.[13] have showed that Mg has a significant influence on the graphite morphology, which causes a substantial increase in nodularity. On one hand, Cu, Si, and Sn only cause change slightly in the nodularity. On the other hand, Cu, Si, and Sn can affect significantly the mechanical properties primarily via altering the pearlite content of a material. Cr and Mo facilitate the formation of carbide and therefore increase the mechanical properties of compacted graphite cast iron. Shy et al.[16] have reported the effects of titanium addition and section size on microstructure and mechanical properties of compacted graphite cast iron. They pointed out that the increasing section sizes facilitate the formation of compacted graphite and ferrite with or without titanium addition. However, alloying with titanium effectively increase both compacted graphite percentage and pearlite content at the same section size. The fracture toughness along with tensile strength of compacted graphite cast irons increase with titanium in all casting sizes. Kim et al.[19] have studied mechanical, wear and weight-loss exposure tests on compacted graphite cast iron of varying nodularity and pearlite percent at elevated temperature. The results showed that the tensile strength at elevated temperature increase linearly and the wear loss decrease slightly with the increasing nodularity and pearlite percent, respectively. Moreover, the heat exposure losses increase with an increase in temperature at the same nodularity and pearlite percent, respectively. Based on aforementioned investigations, it can be inferred that graphite and pearlite content may influence the mechanical properties. Furthermore, the study of thermal conductivity of compacted graphite cast

iron is scarcely. The graphite count is a main influence factor to the thermal conductivity of compacted graphite cast iron. The variation of carbon equivalent can change the graphite count.

Unfortunately, the effects of carbon equivalent on thermal and mechanical properties of compacted graphite cast iron are rarely discussed systematically in current literature. The results are very helpful for further research. Therefore, the present work focus on the effect of carbon equivalent on thermal and mechanical properties of compacted graphite cast iron.

II. MATERIALS AND METHODS

A. Sample preparation of compacted graphite cast iron

The experimental specimens were prepared in a vacuum induction furnace. The furnace charge consisted of the following materials: pig iron, steel scrap, Fe–Mn, Fe–Si, master alloys. After metal heating to a temperature of 1300 °C, and then other master alloys were added. When melt was superheated to 1460 °C, the melt was poured into a Y-type block sand mold (see Fig. 1). For the vermicularizer, the foundry alloy Mg–RE (43–46 wt% Si, 3.5–5.0 wt% Mg, 8–10 wt% RE) with an amount of 0.5 wt% were used. The grain size of vermicularizers ranged from 5 to 6 mm. The inoculation was done by means of the Fe–Si alloy (75% Si) inoculant with an amount of 0.8 wt%. The grain size of inoculants ranged from 8 to 10 mm. Table I shows the chemical compositions of compacted graphite cast iron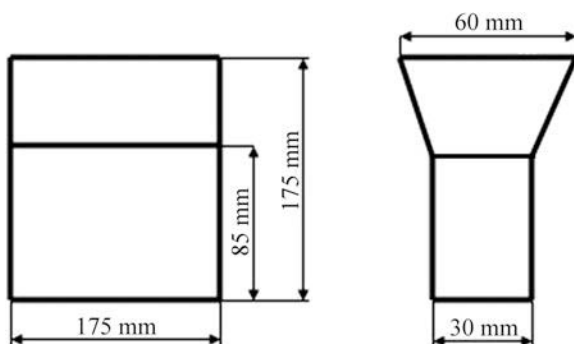s, as analyzed by x-ray fluorescence spectroscopy (LAB CENTER XRF-1800, Shimadzu Corp., Tokyo, Japan). In this Table A1 represents the carbon equivalent about 4.43, A2 refers to the carbon equivalent about 4.52, A3 is the carbon equivalent about 4.64, and A4 represents the carbon equivalent about 4.74. Carbon equivalent was calculated according to the following formula[21]:

$$\text{C.E.} = C\% + 1/3(Si\% + P\%) \qquad (1)$$

B. Thermal conductivity test

A Netzsch LFA 457 laser flash apparatus (Netzsch Group, Selb, Germany) was used to investigate the thermal diffusivity and conductivity, based on the concept developed of Parker et al.[22] The thermal diffusivity, α, and specific heat, C_p, were measured at the temperatures between 20 and 500 °C. The thermal conductivity, λ, was then calculated as follows:

$$\lambda = \alpha \cdot C_p \cdot \rho \quad , \qquad (2)$$

where ρ is the bulk density, α is the thermal diffusivity, and C_p is the specific heat. The unit for λ is W/mK.

C. Mechanical test

Universal testing machine (INSTRON 1342, Britain) was used for tensile testing and tension rate was 1 mm/min. Tensile test specimen was performed obey ASTM-E8M[23] standard, as shown in Fig. 2. Hardness test was also carried out in Brinell hardness tester (HB-3000B, Laizhou Huayin Testing Equipment Co. Ltd., Shandong, China) with a load of 187.5 kg and 10 s duration. All tensile testing was performed in ambient temperature, 300 and 500 °C, respectively. Every data results from the average value of three measurements.

D. Characterization

Optical microscopy (Leica DMI5000M, Germany) was applied to observe graphite morphology and matrix. The percentage of compacted graphite was calculated using the aspect ratio[1] $\left(\text{graphite aspect ratio} = \frac{\text{graphite length}}{\text{graphite width}}\right)$

FIG. 1. Schematic of Y-type block.

TABLE I. Chemical compositions of different carbon equivalent for compacted graphite cast irons (wt%).

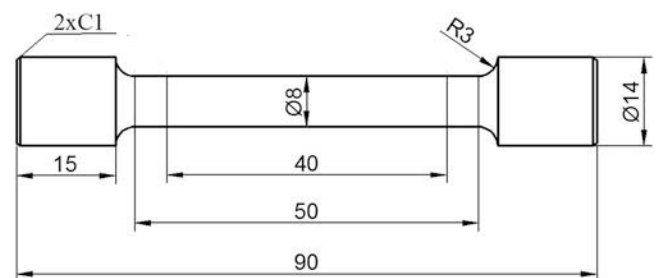| Species	CE	C	Si	Mn	P	S	Cu	Mo	Fe
A1	4.43	3.71	2.12	0.39	0.062	0.033	0.38	0.21	Bal.
A2	4.52	3.79	2.13	0.41	0.058	0.031	0.43	0.22	Bal.
A3	4.64	3.93	2.08	0.43	0.061	0.028	0.41	0.19	Bal.
A4	4.74	4.02	2.12	0.41	0.063	0.034	0.37	0.24	Bal.

FIG. 2. Dimension of tensile specimen.

concept of ASTM A247[24] where a 1:1 ratio is nodular graphite, a ratio of between 1:2 and 1:10 is compacted graphite, and above 1:11 is flake graphite. The matrix was obtained after etching with 4% Nital. Comparing with the photomicrographs to the reference ferrite-pearlite percentage graphs proposed by American Foundrymen's Society Quality Control Committee,[25] the pearlite percentage in the matrix was obtained. The fracture morphology
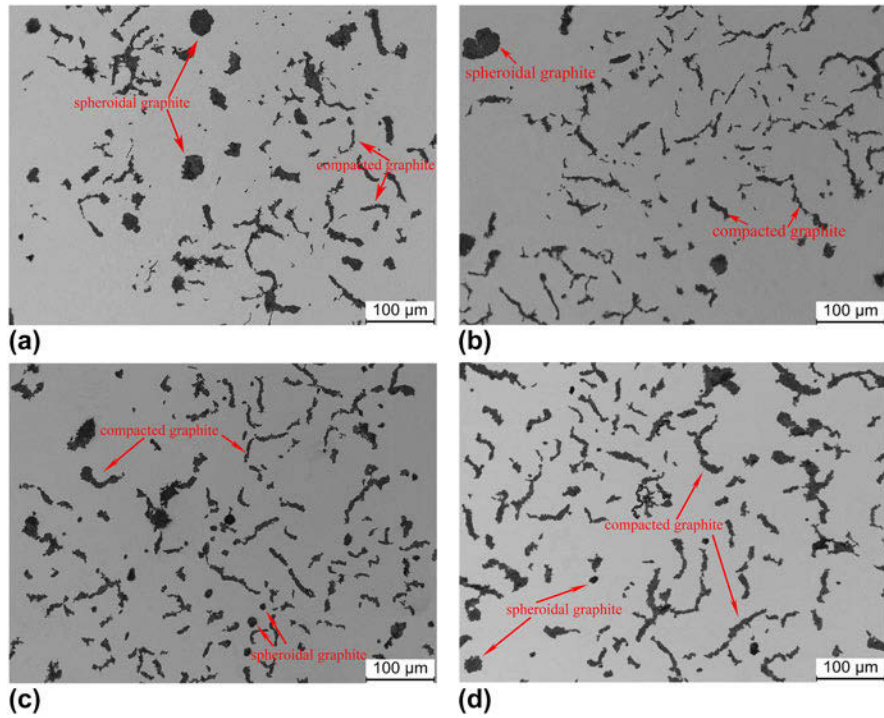

FIG. 3. The graphite morphology of compacted graphite cast irons [(a) A1, (b) A2, (c) A3, (d) A4].
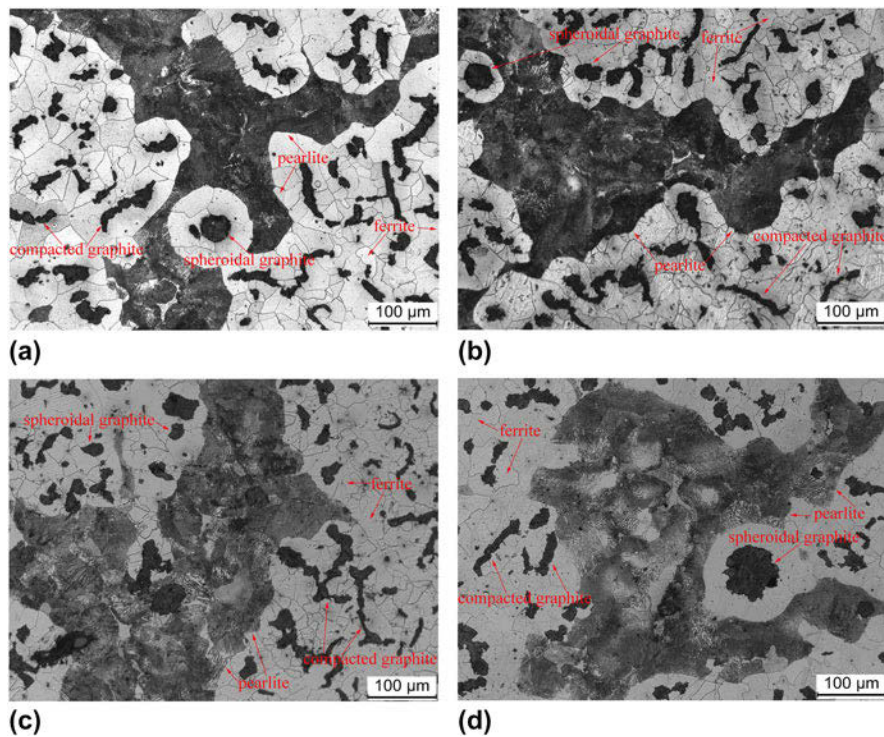

FIG. 4. The matrix structure of compacted graphite cast irons [(a) A1, (b) A2, (c) A3, (d) A4].

of the specimens were carried out using a scanning electron microscope (SEM) (Tescan VEGA II XMU, Brno, Czech Republic) equipped with a secondary electron (SE), performed using an electron accelerating voltage of 20.00 kV.

III. RESULTS AND DISCUSSIONS

A. Microstructures

Figures 3 and 4 show the graphite morphology and the matrix structure of compacted graphite cast irons with different carbon equivalents, respectively. As displayed
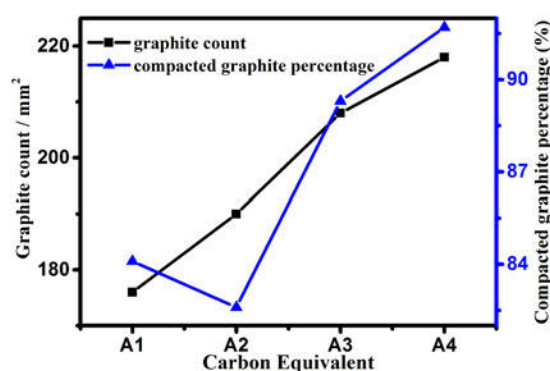

FIG. 5. Effect of carbon equivalent on the graphite count and compacted graphite percentage of compacted graphite cast irons.
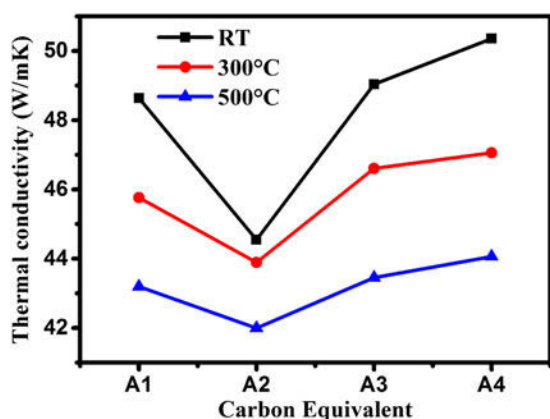

FIG. 6. Thermal conductivity versus carbon equivalent of compacted graphite cast irons at different temperatures.

in Fig. 3, the morphology of graphite is spheroidal and compacted. The increase in graphite results from the increase in carbon equivalent, corresponding to the increase of C-content.[26] Pearlite and ferrite matrix of compacted graphite cast irons, as shown in Fig. 4. The results indicated that the pearlite content increase slightly. The pearlite content of A1, A2, A3, and A4 is 32.91, 33.65, 34.14, and 35.98%, respectively. The percentages of compacted graphite are higher than 80%. Figure 5 shows the variation of graphite count and compacted graphite percentages of compacted graphite cast irons with different carbon equivalents. The graphite count ranges from 176 to 218 (graphite count/mm^2) with A1 to A4. With an increase in carbon equivalent, the compacted graphite percentages decrease initially, and then increase. Generally, the carbon and silicon are the main graphitizing elements.[21] When the silicon is a constant, the higher the carbon equivalent results in the greater the activity of carbon and the stronger graphitization. In other words, the increase of carbon equivalent causes the increase in graphite in cast iron. The increase of graphite count theoretically reduces strength, while the increase of pearlite in matrix enhances strength.[16] How this affected thermal properties and mechanical properties will be further discussed in the following.

B. Thermal properties

Figure 6 shows the thermal conductivities, calculated by Eq. (2), of the compacted graphite cast irons with different carbon equivalents. With an increase in carbon equivalent, the thermal conductivities decrease initially, and then increase at all testing temperature. As the temperature increase from ambient temperature to 500 °C, the thermal conductivity decreased by around 11% from 48.64 to 43.19 W/mK for A1, 6% from 44.55 to 41.99 W/mK for A2, 11% from 49.04 to 43.45 W/mK for A3 and 13% from 50.36 to 44.06 W/mK for A4, respectively. Therefore, for A2, the decrease of thermal conductivity is slighter than others from ambient temperature to 500 °C.

According to the work of Blackmore,[27] the thermal conductivity of metallic matrix structure has little effect on bulk conductivity at different temperatures. Therefore, it can be inferred that the difference in thermal conductivity

TABLE II. Various mechanical properties of compacted graphite cast irons for different carbon equivalents.

	A1			A2			A3			A4		
	RT	300 °C	500 °C	RT	300 °C	500 °C	RT	300 °C	500 °C	RT	300 °C	500 °C
Brinell hardness (HBS)	164.0	…	…	174.5	…	…	168.6	…	…	158.0	…	…
Tensile strength (MPa)	343.5	317.3	223.2	354.3	319.7	227.1	352.8	318.2	226.2	318.6	295.3	194.8
Yield strength (MPa)	281.3	252.1	195.6	292.6	262.2	199.1	291.3	261.1	197.8	273.8	233.3	160.1
Elongation (%)	3.30	4.25	5.53	3.25	3.48	4.52	3.53	3.97	5.38	3.63	4.05	5.63
Yield-tensile ratio	0.82	0.79	0.88	0.83	0.82	0.88	0.80	0.82	0.87	0.86	0.79	0.82

of aforementioned specimens is attributed to the different contents of free graphite in this case. On one hand, the more spheroidal graphite is, the lower the thermal conductivity. Based on the above discussions, the compacted graphite percentage of A2 is lowest. In other word, the spheroidal graphite is higher in A2 than others. Therefore, the thermal conductivity of A2 is lower than others. On the other hand, the compacted graphite is believed to grow alternately in the *c* and *a* direction.
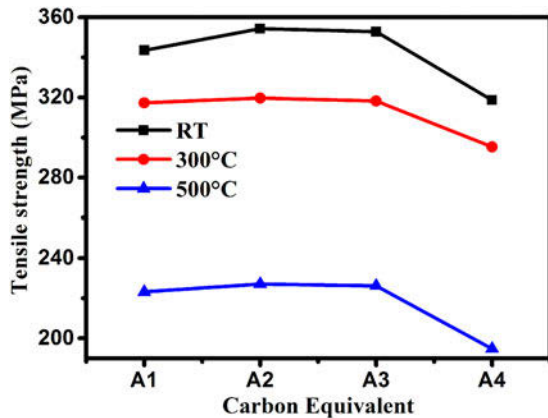

FIG. 7. Effect of different carbon equivalents on tensile strength of compacted graphite cast irons.
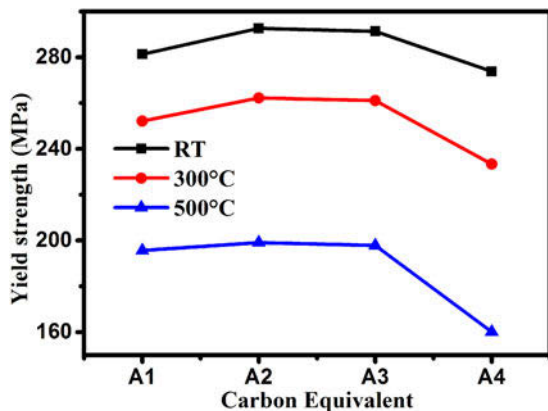

FIG. 8. Variation of yield strength with carbon equivalent of compacted graphite cast irons.

Based on the literature;[28] however, values of around 2000 W/mK along the basal planes and values below 10 W/mK along the prism planes are reported. Thus, the thermal transport properties are significantly dependent on the crystal orientation. As indicated in Fig. 5, the thermal conductivity of A2 is lower than that of A1, while the graphite count of A2 is higher than that of A1. From this, it can be inferred that the prism planes are aligned in the extended directions of graphite at A2. The thermal conductivity of the specimens at A4 is markedly higher than the thermal conductivity of other specimens. This may stem from the highest graphite, higher compacted graphite percentage and its extended directions along with the basal planes at A4.

C. Mechanical properties

Table II shows the mechanical properties of compacted graphite cast irons with different carbon equivalents at different temperatures. It is worth noting that Brinell hardness of compacted graphite cast irons with different carbon equivalents change slightly. This implied that the competing effect between graphite morphology and matrix structure results that Brinell hardness of compacted graphite cast iron is less sensitive to the change of carbon equivalent. Moreover, the yield-tensile ratio of compacted graphite cast irons with different carbon equivalents are greater than 0.8 both at ambient temperature and at high temperature. The results indicated that these compacted graphite cast irons have better resistance to plastic deformation.

Figure 7 compares the tensile strength of compacted graphite cast irons with different carbon equivalents at different temperatures. The tensile strength of compacted graphite cast irons increase initially, and then decrease with an increase in carbon equivalent at different temperatures. The tensile strength of compacted graphite cast irons decrease with an increase in temperature at same carbon equivalent. The highest tensile strength of around 354.3 MPa is obtained at A2 and the lowest one is around 318.6 MPa at A4 at ambient temperature. The more spheroidal graphite is, the higher the tensile strength. Based on aforementioned analyses, the spheroidal graphite
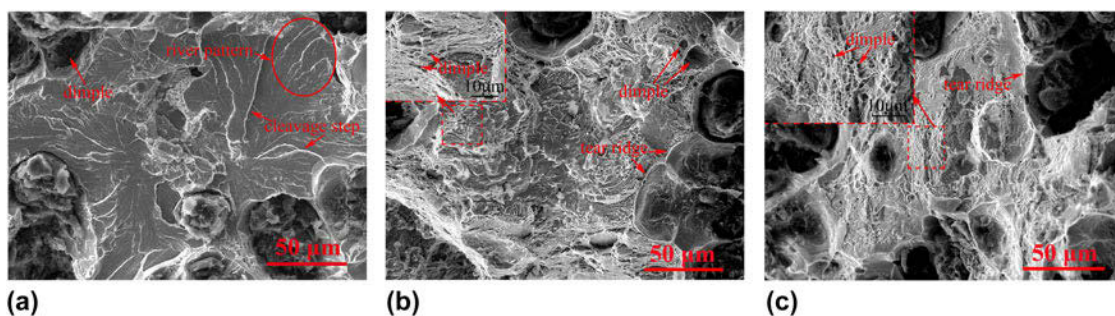

FIG. 9. Fracture surfaces of tensile specimens for A1 at different temperatures: (a) RT, (b) 300 °C, (c) 500 °C.

at A2 is more than others. Therefore, tensile strength at A2 is the highest among all specimens. For A2; however, tensile strength is around 319.7 and 227.1 MPa at 300 °C and 500 °C, respectively, indicating a decline of 9.8% at 300 °C and a sharp decrease by 35.9% at 500 °C. Tensile strength decrease by around 7.6% at 300 °C and 35.0% at 500 °C for A1, 9.8% at 300 °C and 35.9% at 500 °C for A3, 7.3% at 300 °C and 38.9% at 500 °C for A4, respectively. These indicated that the reduction rate of tensile strength of compacted graphite cast irons slightly form ambient temperature to 300 °C, and that of significantly at 500 °C. It is well known that the increase in content of graphite lower the strength, while the increase content of pearlite enhance the strength.[16] The more compacted graphite is, the lower the tensile strength. Moreover, compared with A3, tensile strength of A4

rapidly decreases. The reason for this may be that the sum of graphite and the number of compacted graphite of A4 are higher than A3. The graphite count is the dominant factor causing the variation of tensile strength compared to the content of pearlite in the matrix at A4. The change of tensile strength is more discernible than that of hardness.

Figure 8 shows the yield strength of compacted graphite cast irons as a function of carbon equivalent at different temperatures. The yield strength of compacted graphite cast irons increase initially, and then decrease with an increase in carbon equivalent at different temperatures. With the increasing temperature; however, the yield strength decrease at same carbon equivalent. The yield strength of compacted graphite cast irons decreased by around 30.5% from 281.3 to 195.6 MPa for
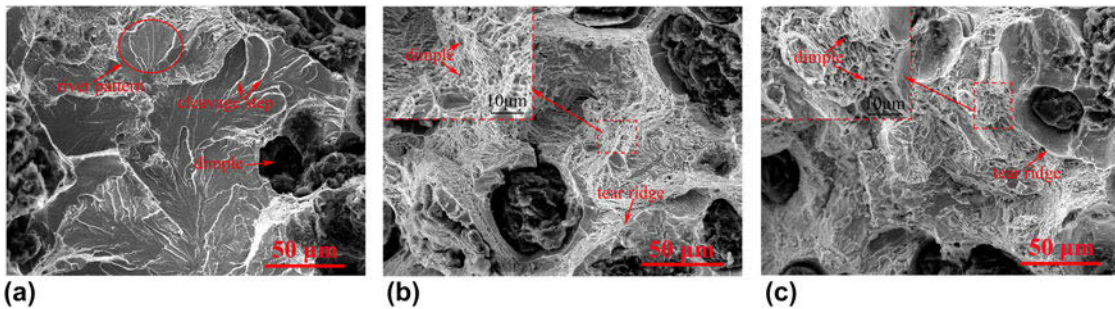

FIG. 10. Fracture surfaces of tensile specimens for A2 at different temperatures: (a) RT, (b) 300 °C, (c) 500 °C.
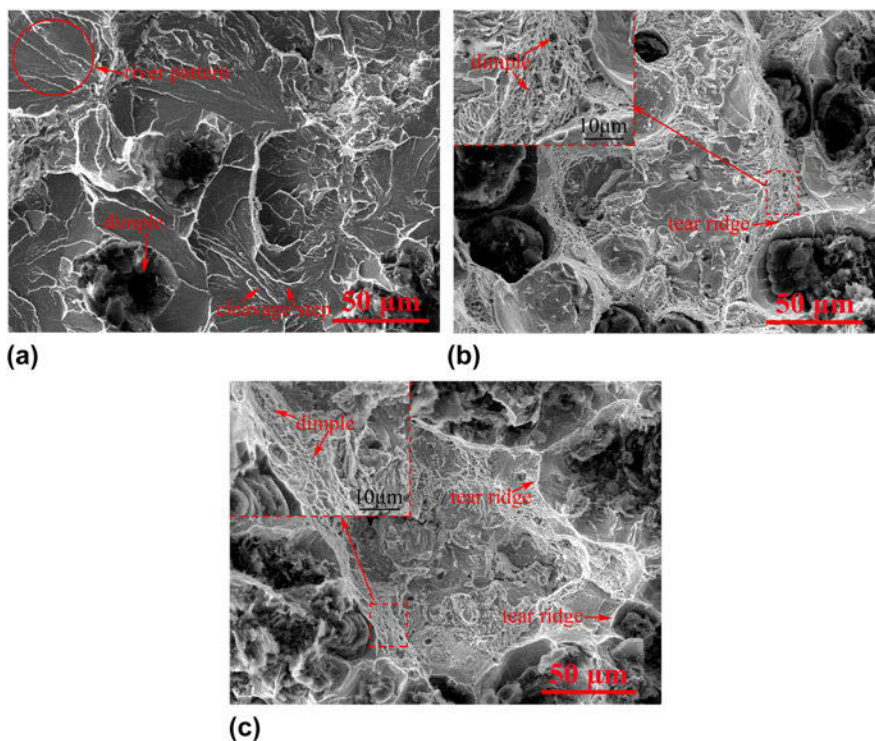

FIG. 11. Fracture surfaces of tensile specimens for A3 at different temperatures: (a) RT, (b) 300 °C, (c) 500 °C.
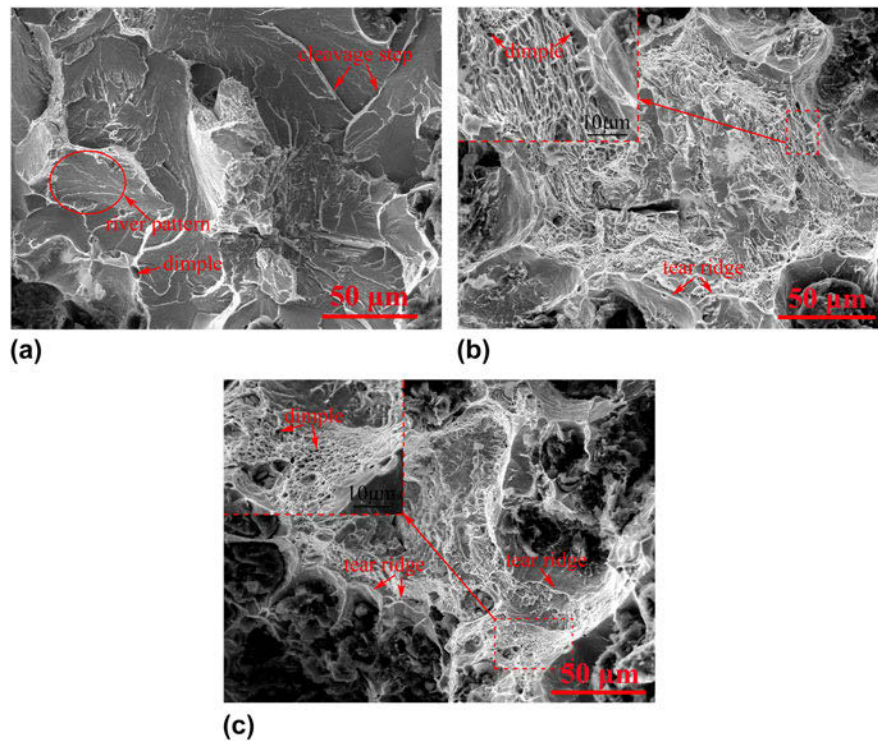
FIG. 12. Fracture surfaces of tensile specimens for A4 at different temperatures: (a) RT, (b) 300 °C, (c) 500 °C.

A1, 31.9% from 292.6 to 199.1 MPa for A2, 32.1% from 291.3 to 197.8 MPa for A3 and 41.5% from 273.8 to 160.1 MPa for A4 with the temperature increase from ambient temperature to 500 °C, respectively. Thus, the yield strength of A4 decreases significantly more than others. This may be that the graphite count and the compacted graphite percentage of A4 is the highest among all specimens, which is the dominant factor to the variation of yield strength at A4.

D. Fractography

Figures 9–12 show the SEM fractographs taken from the broken halves of tensile specimens of compacted graphite cast irons for A1 to A4 at different temperatures. Cleavage step and river pattern are basically micro-characteristics of cleavage fracture. From the Figs. 9(a), 10(a), 11(a), and 12(a), river patterns and cleavage steps are discovered along with cleavage facets. Additionally, the graphite nodules are surrounded by a small amount of dimples. Most of vermicular graphite is fractured. When the force is applied on the specimen, stress concentration forms at the tip of vermicular graphite. Therefore, micro-cracks originate at these places. The micro-cracks without experiencing cavity aggregation growth stage quickly reach at the unstable spreading stage owing to the high stress concentration at the tip of vermicular graphite and the inconsistent deformation ability of ferrite.[29] Cracks spread quickly in the ferrite, which cause cleavage

fracture with flat cleavage plane. Therefore, the brittle cleavage fracture is the main fracture manner of compacted graphite cast irons at ambient temperature. At high temperature, many dimples in the matrix and lower proportion of cleavage surface are found, as shown in Figs. 9(b), 9(c), 10(b), 10(c), 11(b), 11(c) and 12(b), 12(c). The graphite nodules are surrounded by dense dimples, forming tearing ridges. Most of the tearing ridge is closed, as displayed in Figs. 9(b), 9(c), 10(b), 10(c), 11(b), 11(c) and 12(b), 12(c). The close-state of tearing ridges can retard the spread of micro-cracks and the connect of the cracks surround the near graphite nodules.[30] These accounted for the better ductility of compacted graphite cast iron at high temperature. The fracture mechanism can be regarded as: graphite nodules are peeled off from the ferrite under the function of forces and form cavities, the cavities grow up under the effect of slip. Eventually, the cavities connect with each other, which cause the macroscopic fracture. A relatively large plastic deformation of ferrite is generated in this process. Based on the above discussions, the mixed ductile-brittle fracture mode prevailed in compacted graphite cast irons from A1 to A4.

IV. CONCLUSIONS

The effects of carbon equivalent on thermal and mechanical properties of compacted graphite cast irons

at different temperatures were studied. The main conclusions were summarized as follows:

(1) The matrix of the compacted graphite cast irons consisted of pearlite and ferrite, while the morphology of graphite presented spheroidal and compacted. The graphite count increases from A1 to A4. The percentages of compacted graphite for A1 to A4 are higher than 80%.

(2) The thermal conductivity decrease initially, and then increase with an increase in carbon equivalent. The highest and lowest of thermal conductivity is attributed to A4 and A2, respectively. Moreover, with the increasing temperature, the thermal conductivity of compacted graphite cast irons decreases.

(3) The tensile strength and yield strength increase initially, and then decrease with the increasing carbon equivalent at different temperatures, respectively. The hardness has a slight change with the increasing carbon equivalent. The tensile strength and yield strength of compacted graphite cast irons decrease slightly from ambient temperature to 300 °C, respectively. Thereafter, the tensile strength and yield strength decrease significantly at 500 °C, respectively.

(4) The mixed ductile-brittle fracture mode exists in compacted graphite cast irons. At ambient temperature, the brittle cleavage fracture is mainly fracture manner of compacted graphite cast irons. With the increasing temperature, the ductile fracture is mainly fracture mode.

REFERENCES

1. M. Bazdar, H.R. Abbasi, A.H. Yaghtin, and J. Rassizadehghani: Effect of sulfur on graphite aspect ratio and tensile properties in compacted graphite irons. *J. Mater. Process. Technol.* **209**(4), 1701–1705 (2009).

2. M. Górny and M. Kawalec: Effects of titanium addition on microstructure and mechanical properties of thin-walled compacted graphite iron castings. *J. Mater. Eng. Perform.* **22**(5), 1519–1524 (2013).

3. M. Selin, D. Holmgren, and I.L. Svensson: Effect of alloying elements on graphite morphology in CGI. *Mater. Sci. Forum* **649**, 171–176 (2010).

4. S. Dawson and T. Schroeder: Practical applications for compacted graphite iron. *AFS Trans.* **47**(5), 1–9 (2004).

5. J. Liu and N.X. Ding: Effect of type and amount of treatment alloy on compacted graphite produced by the flotret process. *AFS Trans.* **93**, 675–688 (1985).

6. G. Cueva, A. Sinatora, W.L. Guesser, and A.P. Tschiptschin: Wear resistance of cast irons used in brake disc rotors. *Wear* **255**(7), 1256–1260 (2003).

7. G.F. Geier, W. Bauer, B.J. McKay, and P. Schumacher: Microstructure transition from lamellar to compacted graphite using different modification agents. *Mater. Sci. Eng., A* **413**, 339–345 (2005).

8. W. Guesser, T. Schroeder, and S. Dawson: Production experience with compacted graphite iron automotive components. *AFS Trans.* **01–071**, 1–11 (2001).

9. H.Q. Qiu and Z.D. Chen: The forty years of vermicular graphite cast iron development in China (part I). *China Foundry* **4**(2), 91–98 (2007).

10. X. Yang, Z.H. Zhang, J.T. Wang, and L.Q. Ren: Investigation of nanomechanical properties and thermal fatigue resistance of gray cast iron processed by laser alloying. *J. Alloys Compd.* **626**, 260–263 (2015).

11. J.M. Chou, M.H. Hou, and J.L. Lee: Affects of graphite morphology and matrix structure on mechanical properties of cast ions. *J. Mater. Sci.* **25**(4), 1965–1972 (1990).

12. M. Selin, D. Holmgren, and I.L. Svensson: Influence of alloying additions on microstructure and thermal properties in compacted graphite irons. *Int. J. Cast. Met. Res.* **22**(1–4), 283–285 (2009).

13. M. König and M. Wessén: Influence of alloying elements on microstructure and mechanical properties of CGI. *Int. J. Cast. Met. Res.* **23**(2), 97–110 (2010).

14. V. Fourlakidis and A. Diószegi: A generic model to predict the ultimate tensile strength in pearlitic lamellar graphite iron. *Mater. Sci. Eng., A* **618**, 161–167 (2014).

15. H. Pirgazi, S. Ghodrat, and L.A.I. Kestens: Three-dimensional EBSD characterization of thermo-mechanical fatigue crack morphology in compacted graphite iron. *Mater. Charact.* **90**, 13–20 (2014).

16. Y.H. Shy, C.H. Hsu, S.C. Lee, and C.Y. Hou: Effects of titanium addition and section size on microstructure and mechanical properties of compacted graphite cast iron. *Mater. Sci. Eng., A* **278**(1), 54–60 (2000).

17. I. Hervas, M.B. Bettaieb, A. Thuault, and E. Hug: Graphite nodule morphology as an indicator of the local complex strain state in ductile cast iron. *Mater. Des.* **52**, 524–532 (2013).

18. R.A. Gonzaga: Influence of ferrite and pearlite content on mechanical properties of ductile cast irons. *Mater. Sci. Eng., A* **567**, 1–8 (2013).

19. S. Kim, S.L. Cockcroft, A.M. Omran, and H. Hwang: Mechanical, wear and heat exposure properties of compacted graphite cast iron at elevated temperatures. *J. Alloys Compd.* **487**(1), 253–257 (2009).

20. M. Moonesan, A. Honarbakhsh raouf, F. Madah, and A. Habibollah zadeh: Effect of alloying elements on thermal shock resistance of gray cast iron. *J. Alloys Compd.* **520**, 226–231 (2012).

21. H.T. Angus: *Cast Iron: Physical, and Engineering Properties*, 2nd ed. (British Cast Iron Research Association, London, 1978).

22. W.J. Parker, R.J. Jenkins, C.P. Butler, and G.L. Abbott: Flash method of determining thermal diffusivity, heat capacity, and thermal conductivity. *J. Appl. Phys.* **32**(9) 1679–1784 (1961).

23. ASTM E8M-91: *Annual Book of ASTM Standards*, 1986 (ASTM International, West Conshohocken, 1986); pp. 637–644.

24. ASTM A247-67: *Annual Book of ASTM Standards*, 1990 (ASTM International, West Conshohocken, 1990); pp. 129–130.

25. E.F. Ryntz, Jr: Prediction of nodular iron microstructure using thermal analysis. *AFS Trans.* **79**, 141–144 (1971).

26. N. Fatahalla, A. Abuelezz, and M. Semeida: C, Si and Ni as alloying elements to vary carbon equivalent of austenitic ductile cast iron: Microstructure and mechanical properties. *Mater. Sci. Eng., A* **504**(1), 81–89 (2009).

27. P.A. Blackmore and K. Morton: Structure-property relationships in graphitic cast irons. *Int. J. Fatigue* **4**(3), 149–155 (1982).

28. D. Holmgren, R. Källbom, and I.L. Svensson: Influences of the graphite growth direction on the thermal conductivity of cast iron. *Metall. Mater. Trans. A* **38**(2), 268–275 (2007).

29. I. Asenjo, P. Larranaga, and J. Sertucha: Effect of mould inoculation on formation of chunky graphite in heavy section spheroidal graphite cast iron parts. *Int. J. Cast. Met. Res.* **20**(6), 319–324 (2007).

30. M. König: Literature review of microstructure formation in compacted graphite iron. *Int. J. Cast. Met. Res.* **23**(3), 185–192 (2010).